

Variability of Threshold Voltage Induced by Work-Function Fluctuation and Random Dopant Fluctuation on Gate-All-Around Nanowire nMOSFETs

Wen-Li Sung
Department of Electrical and
Computer Engineering,
Center for mmWave Smart Radar
System and Technologies,
National Chiao Tung University,
Hsinchu 30010, Taiwan.

Min-Hui Chuang
Department of Electrical and
Computer Engineering,
Center for mmWave Smart Radar
System and Technologies,
National Chiao Tung University,
Hsinchu 30010, Taiwan.

Yiming Li
Department of Electrical and
Computer Engineering,
Center for mmWave Smart Radar
System and Technologies,
National Chiao Tung University,
Hsinchu 30010, Taiwan.
Email: ymli@faculty.nctu.edu.tw

Abstract—We advance the localized work-function fluctuation (LWKF) method to examine the variability of threshold voltage (V_{th}) induced by titanium nitride (TiN) metal-gate work-function fluctuation (WKF) and combined the WKF with the random dopant fluctuation (RDF) for various grain sizes on Si gate-all-around (GAA) nanowire (NW) MOSFETs. Our results show that the WKF-induced variability of V_{th} will be dominated by bamboo-type TiN grains and its impact is larger than that induced by the RDF with doped channel (RDF (doped)). Additionally, the variability of V_{th} induced by the WKF and the RDF (doped) could be treated as independent fluctuation sources because the channel dopants are away from the metal-gate/high- κ interface. Consequently, statistical models are further proposed for the σV_{th} induced by the WKF and the combined WKF with RDF (doped) by considering position effect of nanosized TiN grains.

Keywords—GAA; Nanowire; TiN; Work function fluctuation; Random dopant fluctuation; Grain size; Statistical model.

I. INTRODUCTION

Nano-sized nanowire (NW) metal-oxide semiconductor field-effect transistors (MOSFETs) with high- κ /metal gate technology become an attractive device to replace the fin field-effect transistors (FinFETs) for sub-5-nm technological nodes due to better electrical characteristics [1]-[3]. However, the crystal orientation of nanosized metal grains is hard to control during the high temperature process in relative smaller gate area [4]-[5]. This will cause the variability of V_{th} owing to different value of work function at the metal-gate/high- κ interface. It was reported that the WKF-induced V_{th} variability for various metal materials can be modeled below by using the average WKF (AWKF) method [6]:

$$\sigma_{th} = A_{VT}(GS/A)^{0.5}, \quad (1)$$

where GS is the average grain size and A is the metal gate area, and A_{VT} (mV) is a fitting factor depending on various metals. However, the AWKF method did not consider the random position effect of metal grains and it will underestimate the

impact of WKF-induced variability of V_{th} [7]. Thus, in this study, the LWKF method is further advanced to estimate the variability of V_{th} considering the location effect for exact grain size ratio ($GSR = GS/A$). Explicit statistical expressions for the σV_{th} are then discussed.

II. STATISTICAL DEVICE SIMULATION METHOD

Figure 1(a) illustrates the schematic of the GAA NW device with various types of RDDs that are statistically generated by the Monte Carlo (MC) method [9]. The simulated structure consists of a metal-gate (TiN)/high- κ (HfO_2) stack with cylindrical Si channel, where the effective work-function (WK) of the TiN metal is set to be 4.552 eV, the gate length is 10 nm, the radius of cylindrical channel is 5 nm, and the effective oxide thickness is 0.6 nm. The various RDDs are generated by the equivalent channel doping concentration with $5 \times 10^{17} \text{ cm}^{-3}$, the equivalent S/D extension doping concentration with $5 \times 10^{18} \text{ cm}^{-3}$, and dopants concentrations with $3.36 \times 10^{17} \text{ cm}^{-3}$ resulting from the penetration of the S/D extension, respectively [9]. Fig. 1(b) shows a flow chart of LWKF method. First, metal gate is partitioned by different grain sizes. Then, we set different WK and probability (p) in the MC program for different metal grain orientations: TiN<200> ($p = 0.6$, WK = 4.63 eV) and TiN<111> ($p = 0.4$, WK = 4.43 eV), respectively [10]. Finally, we generate 200 fluctuated 3D devices with different grain sizes by the MC program to explore the effect of the WKF and combined the WKF and RDF (doped) on the device variability.

III. RESULTS AND DISCUSSION

Figure 2 presents the cumulative probability of V_{th} induced by the RDF, the WKF, and the combined WKF and RDF with doped channel. It is obvious that the distributions of V_{th} with these simulation conditions were close to Gaussian and continuous distribution. However, it differs from other researcher's results with uniformly square grain pattern method

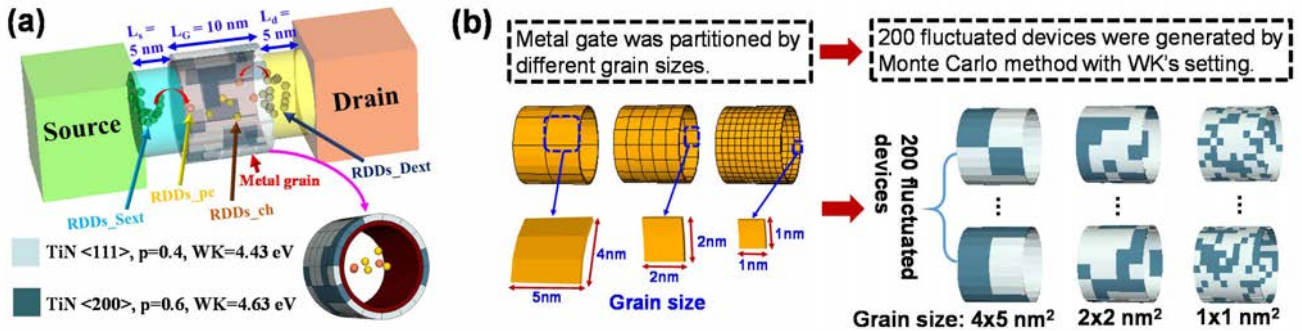


Fig. 1. (a) Schematic of the GAA NW device with various types of RDDs and metal grains, where the gate length is 10 nm, the radius of cylindrical channel is 5 nm, and the effective oxide thickness is 0.6 nm [9]. (b) Flow chart of LWKF method, which partitioned by three grain sizes in the same metal gate area.

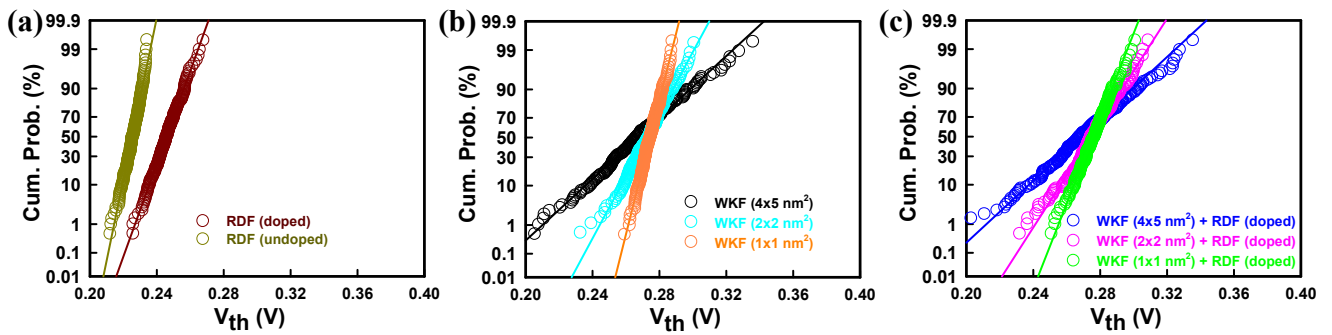


Fig. 2. The cumulative probability of V_{th} . (a) RDF, (b) WKF, and (c) Combined WKF with RDF (doped).

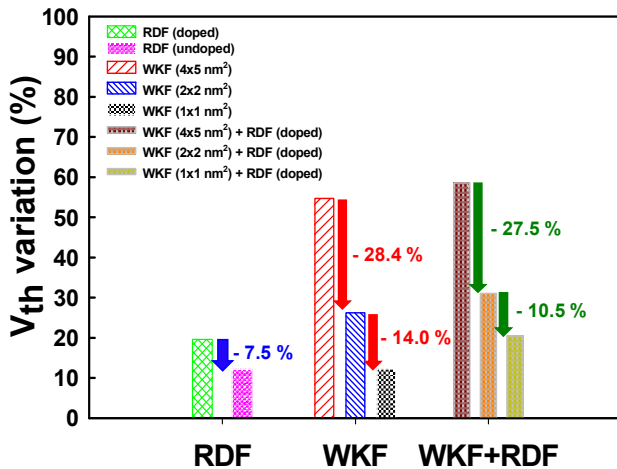


Fig. 3. The V_{th} variation induced by the RDF, the WKF and the combined WKF with RDF (doped), respectively.

[11]. As indicated in Fig. 2(a), the slope of the V_{th} distribution induced by doped channel was smaller than that of the undoped channel condition. The results indicate that the V_{th} variation can be improved without channel doping for the RDF simulation. Fig. 2(b) shows the distribution of V_{th} induced by the WKF with different grain size patterns. It is observed that the grain size increases, the slope of the V_{th} distribution increases in value. It means that the reduction of the V_{th} variation can be controlled by smaller grain size. We will further discuss the grain size

effect by the GSR from statistical perspective later. Similarly, the distribution of V_{th} induced by the combined WKF and RDF with doped channel, as shown in Fig. 2(c), has the same trend as compared to Fig. 2(b).

To estimate and compare the impact of the V_{th} variation induced by the RDF, the WKF and the combined WKF and RDF with doped channel, we normalized the V_{th} variation by $(6\sigma/\text{mean}) \times 100\%$, where σ is the standard deviation of the characteristic parameters, and mean is the average of the characteristic parameters. Fig. 3 shows the V_{th} variation induced by the RDF, the WKF and the combined WKF and RDF with doped channel, respectively. The reduction of the V_{th} variation induced by the RDF with undoped channel is 7.5%, as compared to the RDF with doped channel. It is smaller than the cases of the WKF (the total reduction rate is the sum of 28.4% and 14.0%) and the combined WKF and RDF with doped channel (the total reduction rate is the sum of 27.5% and 10.5%). In contrast, the V_{th} variation (54.66%) induced by the WKF with largest grain size (bamboo-type grain structure) in our simulation has larger variation than that induced by the RDF with doped channel (19.63%). While the WKF with grain size is below 4 nm², the V_{th} variation induced by the RDF with doped channel will be comparable to that induced by the WKF (12.24% ~ 26.2%). This implies that the grain size effect induced by the WKF may be larger than that the random-discrete doping effect in the channel.

To analyze the grain size effect and statistically empirical equations, we employ the GSR to an x-axis [12]-[13] for the plot

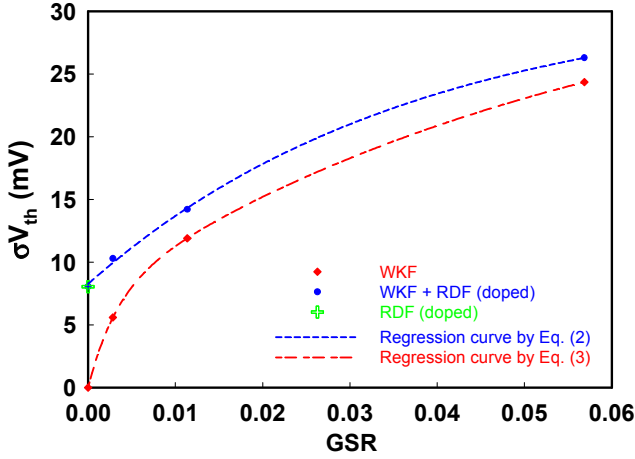


Fig. 4. Plot of the σV_{th} versus GSR, where the blue circle dot is the σV_{th} induced by WKF + RDF (doped channel), the red diamond dot is the σV_{th} induced by WKF, the green cross is the σV_{th} induced by the RDF (doped), the blue short-dash line is the regression curve by Eq. (2) and the red short-long line is the regression curve by Eq. (3).

of the standard deviation of the V_{th} (σV_{th}) versus GSR, as shown in Fig. 4. We consider the range of the GSR in the x-axis from 0 to 0.06 (i.e., from the amorphous-type to the bamboo-type grain structure) in our simulation. First, we apply the non-linear regression curves to fit the simulation results by the optimized method. Because of uniformly square grain size method in this simulation, the value of the GSR is exactly plot in the x-axis. Thus, we only consider the sum of squares of residuals for y-axis (σV_{th}). Moreover, we assume that the data points are independent and statistical noise-free. Then, we try to employ the following empirical Eq. (2) and Eq. (3) to fit the curves of σV_{th} versus GSR induced by the combined WKF and RDF with doped channel, and the WKF, respectively, due to best correlation coefficient (the values of the R^2 are close to 1).

$$\sigma V_{th_RDF+WKF} = \sigma V_{th_RDF} + a \times (1 - e^{-b \times GSR}) \quad (2)$$

$$\sigma V_{th_WKF} = a \times (1 - e^{-b \times GSR}) + c \times (1 - e^{-d \times GSR}), \quad (3)$$

where the a, b, c, and d are the extracted parameters.

At the GSR = 0, as shown in Table I, the value of the σV_{th_RDF} in Eq. (2) is close to the value of the σV_{th} (8.05 mV) induced by the RDF with the doped channel (green cross). To analyze the different regions of the GSR for grain size effect, we differentiate the Eq. (2) and Eq. (3) to obtain the slopes of the curves for the whole GSR, respectively, as following equations:

$$\frac{d(\sigma V_{th_RDF+WKF})}{d(GSR)} = a \times b \times (e^{-b \times GSR}) \quad (4)$$

$$\frac{d(\sigma V_{th_WKF})}{d(GSR)} = a \times b \times (e^{-b \times GSR}) + c \times d \times (e^{-d \times GSR}) \quad (5)$$

For smaller grain size (i.e., the GSR is below 0.01), we apply the Taylor's expansion to Eq. (2) and Eq. (3), respectively. We can find the linear relationship between the σV_{th} and the GSR, where the parameters $\{a \times b\}$ for Eq. (2) and $\{a \times b + c \times d\}$ for Eq. (3) are the slopes of the linear equations, respectively. Many research groups in the world-wide also found this linear behavior [11]-[13]. Furthermore, the slopes will determine the

Table I. The extracted parameters from Eq. (2) and Eq. (3).

Equation	σV_{th_RDF}	a	b	c	d
Eq. (2)	8.27	23.0	26.8	0	0
Eq. (3)	0	72.6	31.6	27.5	17.1

changing rate of the V_{th} variation according to Eq. (4) and Eq. (5). As the GSR increases, the slopes decrease due to exponential decay factor. In the smaller GSR, the slope of the combined WKF and RDF with doped channel is smaller than that of the WKF. It implies that the impact of the V_{th} variation induced by the RDF with doped channel is comparable to that of the WKF for smaller grain size. The slopes may be dominated by the metal orientations of various materials that depend on the different generated probabilities. Thus, various metal materials or composited metal materials may alter the behavior of the V_{th} variation induced by the WKF. For the larger GSR (> 0.01), the curve of the σV_{th} versus the GSR will become linear-like saturation [11]-[13] and it is controlled by the asymptote parameter $\{a\}$ or $\{c\}$. Although the freedom of data points will influence the extracted parameters, fitting curves and 95% confidence intervals, based on our simulation results and other researchers' results [11]-[13], we believe that the non-linear empirical equations in our study is one of best ways to describe the metal grain size effect in our limited knowledge. Finally, the WKF and the RDF can be viewed as independent fluctuation sources since the statistical sum of the WKF with the RDF (doped) can be approximated by Eq. (6) due to the dopants away from the TiN/HfO₂ interface.

$$\sigma V_{th_RDF+WKF} = \sqrt{(\sigma V_{th_RDF})^2 + (\sigma V_{th_WKF})^2}. \quad (6)$$

IV. CONCLUSIONS

In summary, we have found that the grain size/metal gate area and location of metal grains are critical to suppress the variability of V_{th} . The smaller grain size will have a smaller V_{th} variation induced by the WKF. For comparison of the impact of the WKF and the RDF, the results show that the V_{th} variation (54.66%) induced by the WKF with largest grain size (bamboo-type grain structure) has larger impact than that induced by the RDF with doped channel (19.63%). If the GSR is larger than 0.01, the grain size effect induced by the WKF will be more important than that induced by the random-discrete doping effect in the channel. And, according to statistically non-linear empirical equations in our study, in the smaller GSR region, the curves of the σV_{th} versus the GSR will be linear relationship. The changing rate of the σV_{th} are depending on the slopes of the curves. In larger GSR region, the curves of the σV_{th} versus the GSR become linear-like saturation. Moreover, the slopes of the fitting curves may be influenced by the distribution of metal orientations with different materials. The statistical models of σV_{th} offer a new perspective relating to grain size, metal gate area, and different metal-gate materials for sub-5-nm technological nodes.

ACKNOWLEDGMENT

This work was supported in part by the Ministry of Science and Technology, Taiwan, under Grant MOST 106-2221-E-009-149, Grant MOST 106-2622-8-009-013-TM, Grant MOST 107-2622-8-009-011-TM, Grant MOST 107-2221-E-009-094, and Grant MOST 107-3017-F-009-001, in part by the “Center for mmWave Smart Radar Systems and Technologies” under the Featured Areas Research Center Program within the framework of the Higher Education Sprout Project by the Ministry of Education in Taiwan.

REFERENCES

- [1] J. Appenzeller, J. Knoch, M. T. Björk, H. Riel, H. Schmid, and W. Riess, “Toward nanowire electronics,” *IEEE Trans. Electron Devices*, vol. 55, no. 11, pp. 2827–2845, Nov. 2008, doi: 10.1109/TED.2008.2008011.
- [2] H. Mertens, R. Ritzenthaler, V. Pena1, G. Santoro1, K. Kenis, A. Schulze, E. D. Litta, S. A. Chew, K. Devriendt, T. Chiarella, S. Demuyneck, D. Yakimets, D. Jang, A. Spessot, G. Eneman, A. Dangol, P. Lagrain, H. Bender, S. Sun, M. Korolik, D. Kioussis, M. Kim, K.-H. Bu, S. C. Chen, M. Cogorno, J. Devrajan, J. Machillot, N. Yoshida, N. Kim, K. Barla, D. Mocuta, N. Horiguchi, “Vertically stacked gate-all-Around Si nanowire transistors: key process optimizations and ring oscillator demonstration,” in *IEDM Tech. Dig.*, pp.828–831, 2017, doi: 10.1109/IEDM.2017.8268511.
- [3] H. Mertens, R.S. Barraud, V. Lapras, B. Previtali, M.P. Samson, J. Lacord, S. Martinie, M.-A. Jaud, S. Athanasiou, F. Triozon, O. Rozeau, J.M. Hartmann, C. Vizioz, C. Comboroure, F. Andrieu, J.C. Barbé, M. Vinet, and T. Ernst, “Performance and design considerations for gate-all-around stacked-nanowires FETs,” in *IEDM Tech. Dig.*, pp.677–680, 2017, doi: 10.1109/IEDM.2017.8268473.
- [4] M. M. Hussain1, M. A. Quevedo-Lopez1, H. N. Alshareef, H. C. Wen, D. Larison, B. Gnade and M. El-Bouanani, “Thermal annealing effects on a representative high-k/metal film stack,” *S. S. Technol.*, vol. 21, no. 10, pp. 1437-1440, 2006, <https://iopscience.iop.org/article/10.1088/0268-1242/21/10/012>.
- [5] J.L. He, Y. Setsuhara, I. Shimizu, S. Miyake, “Structure refinement and hardness enhancement of titanium nitride films by addition of copper,” *Surf. Coat. Technol.*, vol. 137, pp. 38-42, 2001, [https://doi.org/10.1016/S0257-8972\(00\)01089-6](https://doi.org/10.1016/S0257-8972(00)01089-6).
- [6] C.-H. Yu et al., “Statistical Simulation of Metal-Gate Work-function Fluctuation in High-/Metal-Gate Devices,” in *Proc. SISPAD, 2010*, pp. 153–156, doi: 10.1109/SISPAD.2010.5604544.
- [7] H.-W. Cheng and Y. Li, “Random Work Functions Induced DC and Dynamic Characteristic Fluctuations in 16-nm High-κ/Metal Gate CMOS Device and Digital Circuit,” in *ASQED*, pp. 203-206, 2011, doi: 10.1109/ASQED.2011.6111745.
- [8] Y. Li, H.-T. Chang, C.-N. Lai, P.-J. Chao, and C.-Y. Chen, “Process variation effect, metal-gate work-function fluctuation and random dopant fluctuation of 10-nm gate-all-around silicon nanowire MOSFET devices,” in *IEDM Tech. Dig.*, pp. 887–890, Dec. 2015, doi: 10.1109/IEDM.2015.7409827.
- [9] W.-L. Sung and Y. Li, “DC/AC/RF characteristic fluctuations induced by various random discrete dopants of gate-all-around silicon nanowire n-MOSFETs,” *IEEE Trans. Electron Devices*, vol. 65, no. 6, pp. 2638-2646, Jun. 2018, doi: 10.1109/TED.2018.2822484.
- [10] A. Yagishita, T. Saito, K. Nakajima, S. Inumiya, K. Matsuo, T. Shibata, Y. Tsunashima, K. Suguro, and T. Arikado, *IEEE Trans. Electron Devices*, vol. 48, no. 8, pp. 1604–1611, 2001, doi: 10.1109/16.936569.
- [11] S.-H. Chou, M.-L. Fan, and P. Su, “Investigation and comparison of work function variation for FinFET and UTB SOI devices using a voronoi approach,” *IEEE Trans. Electron Devices*, vol. 60, no. 4, pp. 1485–1489, Apr. 2013, doi: 10.1109/TED.2013.2248087.
- [12] D. Nagy, G. Indalecio, A. J. Garcia-Loureiro, M. A. Elmessary, K. Kalna, and N. Seoane, “Metal grain granularity study on a gate-all-around nanowire FET,” *IEEE Trans. Electron Devices*, vol. 64, no. 12, pp. 5263–5269, 2017, doi: 10.1109/TED.2017.2764544.
- [13] H. Nam, Y. Lee, J.-D. Park, and C. Shin, “Study of work-function variation in high-κ/metal-gate gate-all-around nanowire MOSFET,” *IEEE Trans. Electron Devices*, vol. 63, no. 8, pp. 3338–3341, Aug. 2016, doi: 10.1109/TED.2016.2574328.